# Supporting Information

# Selective Enriching of Trionic Emission in a $WS_2$-ZnO Hybrid through Type-II Band Alignment

*Jin Feng LEONG[1], Kim Yong LIM[1], Xiao WU[2], Qing Hua XU[2], Chorng Haur SOW[1], Eng Tuan POH[1*]*

[1]Department of Physics, National University of Singapore, 2 Science Drive 3, Singapore 117551

[2]Department of Chemistry, National University of Singapore, 3 Science Drive 3, Singapore 117543

*E-mail: phyetp@nus.edu.sg

Table S1: Benchmark table across multiple substrates for trion enhancement in monolayer $WS_2$

| | Laser power density ($MW/cm^2$) | $I_{exciton}/I_{trion}$ |
|---|---|---|
| Suspended/Free-standing[1] | 0.01 | 1:0.25 |
| $Al_2O_3$[2] | 0.3 | 1:0.62 |
| Au[2] | 0.3 | 1:0.42 |
| hBN[3] | 0.24 | 1:0.0375 |
| Graphene[4] | -* | 1:0 |
| $SiO_2$ (Our work) | 0.01 | 1:0.44 |
| ZnO (Our work) | 0.01 | 1:0.54 |
| ZnO (Our work) | 0.1 | 1:1.09 |

*While this work did not indicate the laser power used, they did present a reference $WS_2$ sample on $SiO_2$/Si, which shows trion to exciton ratio of ~1:0.25. Assuming that the laser power used to measure both samples are the same, we can deduce that the trion emission should be quenched by graphene.

Reference

[1] Harats M G et al., Kirchhof J N et al., Qiao M et al. Dynamics and efficient conversion of excitons to trions in non-uniformly strained monolayer $WS_2$, Nat. Pho., 2020, 14, 324–329.

[2] Das S et al., Chowdhury R K et al., Karmakar D et al. Substrate-dependent synergistic many-body effect in atomically thin two-dimensional $WS_2$, Phys. Rev. Materials, 2021, 5, 124001.

[3] Yusuke H et al., Kuroda T et al., Okada M et al. Suppression of exciton-exciton annihilation in tungsten disulfide monolayers encapsulated by hexagonal boron nitride, Phys. Rev. B, 2017, 95, 241403.

[4] Kobayashi Y et al., Sasaki S et al., Mori S et al. Growth and Optical Properties of High-Quality Monolayer $WS_2$ on Graphite, ACS Nano., 2015, 9(4), 4056–4063.

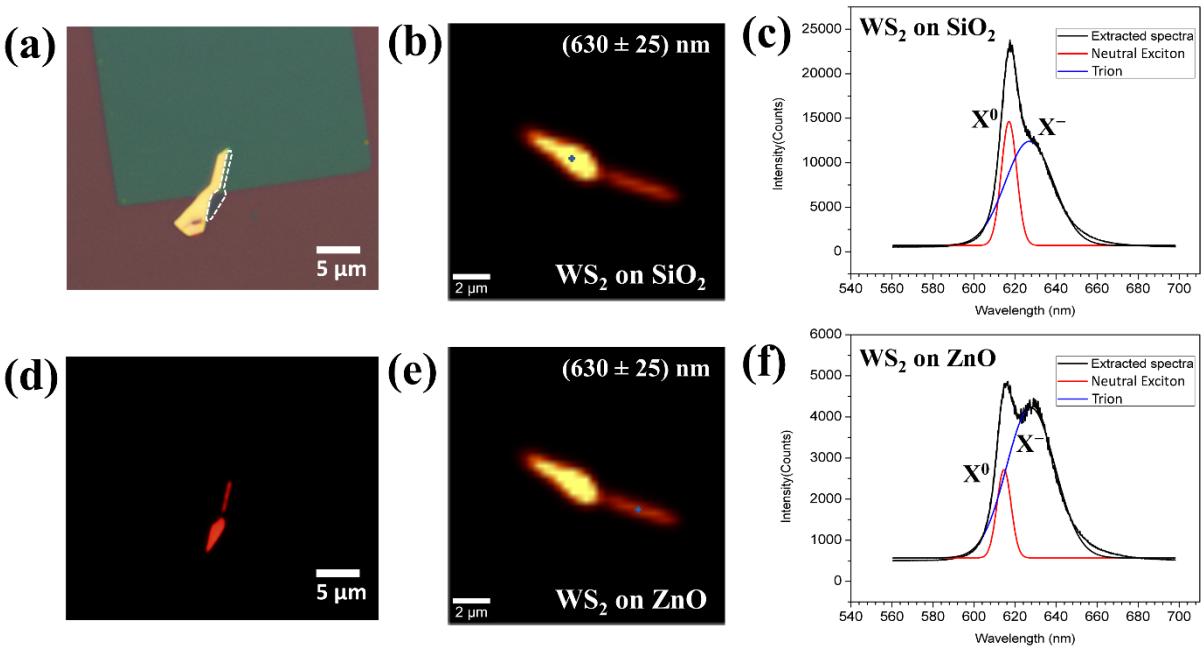


**Figure S1. Reproducibility Test and Characterization Upon A Second $WS_2$-ZnO Heterostructure. (a)** Optical microscopy image of the $WS_2$-ZnO heterostructure formed from exfoliated $WS_2$ placed onto a ZnO square film. **(b)** PL map of the fluorescence distribution for the monolayer region over (630 ± 25) nm, with the marked-out spot location corresponding to the spectrum acquired in **(c)**. **(c)** PL spectrum for the $WS_2$ on $SiO_2$ spot marked in **(b)**, deconvoluted of the exciton trion components. **(d)** Fluorescence micrograph demonstrating the uniform emission distribution over the monolayer region of the sample. **(e)** PL map of the fluorescence distribution for the monolayer region over (630 ± 25) nm, with the marked-out spot location corresponding to the spectrum acquired in **(f)**. **(f)** PL spectrum for the $WS_2$ on ZnO spot marked in **(e)**, demonstrating the increased trion contribution.

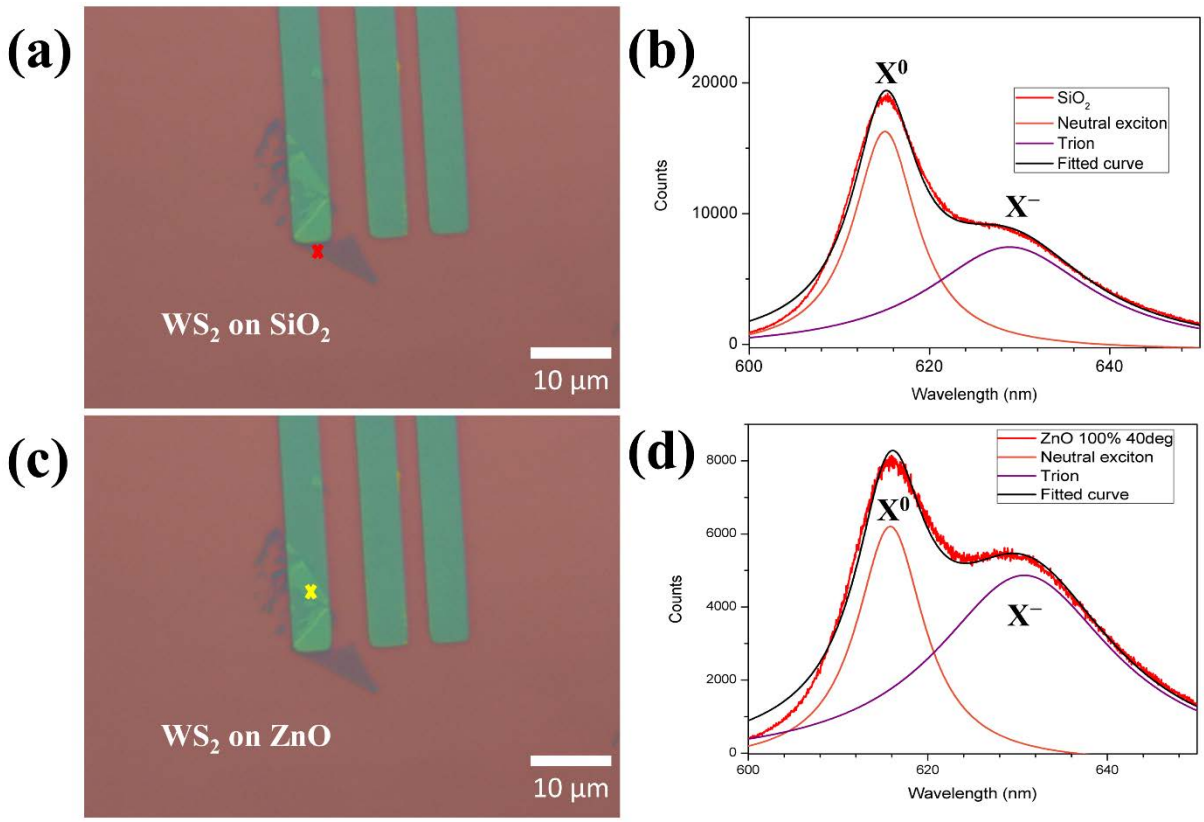


**Figure S2. Reproducibility Test and Characterization Upon A Third $WS_2$-ZnO Heterostructure.** **(a)** Optical microscopy image of the $WS_2$-ZnO heterostructure constructed upon emplacement of the exfoliated $WS_2$ atop the ZnO finger array. Spot marked with red "x" corresponds to where the PL spectrum in **(b)** was acquired from. **(b)** PL spectrum for the $WS_2$ on $SiO_2$ spot marked in **(a)**, deconvoluted of the exciton trion components. **(c)** Optical microscopy image of the $WS_2$-ZnO heterostructure constructed upon emplacement of the exfoliated $WS_2$ atop the ZnO finger array. Spot marked with yellow "x" corresponds to where the PL spectrum in **(d)** was acquired from. **(d)** PL spectrum for the $WS_2$ on ZnO spot marked in **(c)**, demonstrating the increased trion contribution.

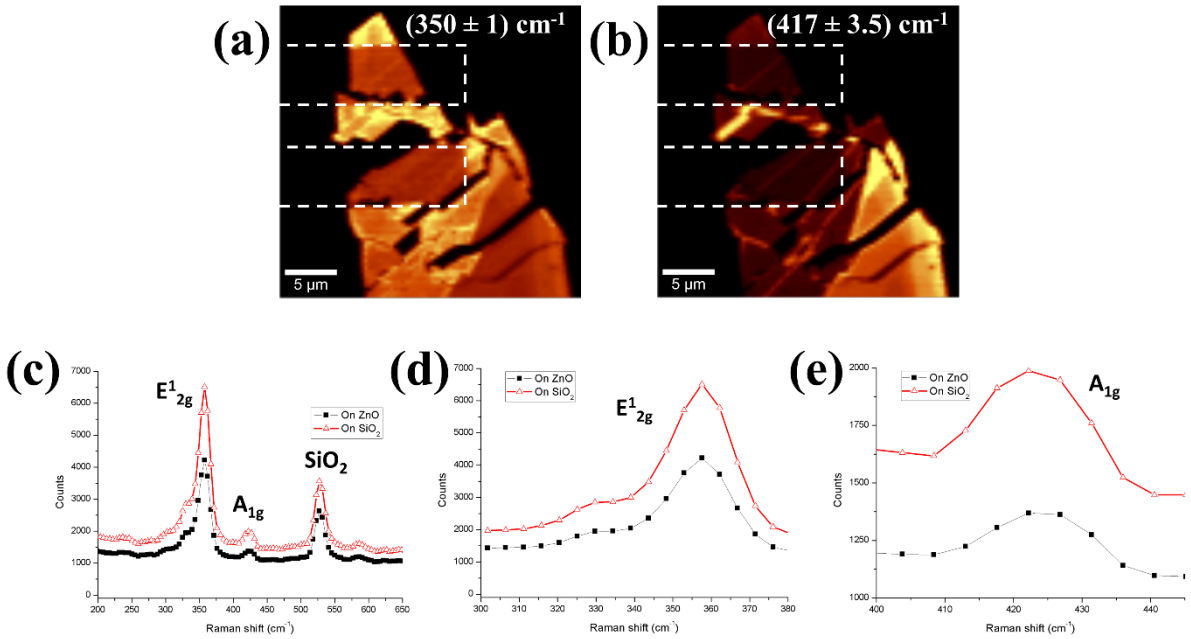


**Figure S3. Raman Characteristics of the $WS_2$-ZnO Heterostructure.** **(a)** Raman mapping across the heterostructure domain spanning the wavenumber range of (350 ± 1) $cm^{-1}$, corresponding to the $E^1_{2g}$ phonon active mode of $WS_2$ in-plane vibration. **(b)** Raman mapping across the heterostructure domain spanning the wavenumber range of (417 ± 3.5) $cm^{-1}$, corresponding to the $A_{1g}$ phonon active mode of $WS_2$ out-of-plane vibration. **(c)** Overall Raman spectra comparison for $WS_2$ on $SiO_2$ and $WS_2$ on ZnO, detailing the $E^1_{2g}$, $A_{1g}$ and $SiO_2$ peaks. **(d)** Magnified Raman spectra feature around $E^1_{2g}$ signal, detailing the difference in peak intensity for the $WS_2$ samples on the different substrates. **(e)** Magnified Raman spectra feature around $A_{1g}$ signal, detailing the difference in peak intensity for the $WS_2$ samples on the different substrates.

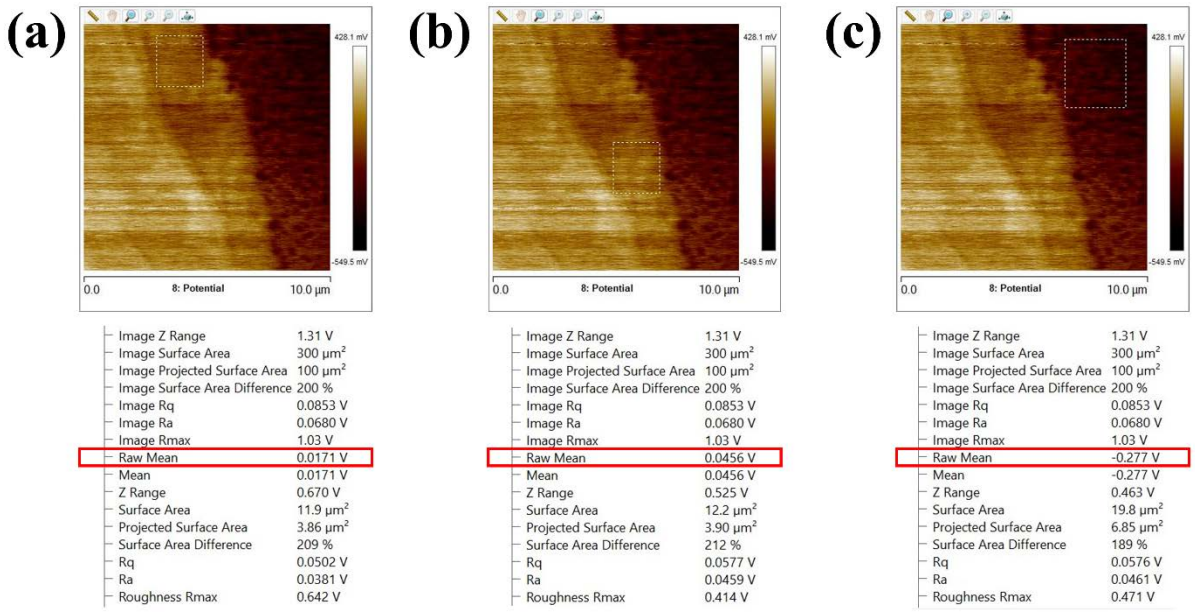


**Figure S4. KPFM Statistics for the $WS_2$-ZnO Heterostructure at Different Sample Domains. (a)** Averaged measurement details for $WS_2$ on Si sample region marked by dashed white square in the KPFM scan map. **(b)** Averaged measurement details for $WS_2$ on ZnO overlay heterostructure region marked by dashed white square in the KPFM scan map. **(c)** Averaged measurement details for ZnO on Si sample region marked by dashed white square in the KPFM scan map. Red rectangular outlines in the measurement statistics highlight the contact potential difference (CPD) acquired for each sample zone with respective to the applied tip potential. The relative sample work function can be acquired from the difference in CPD between $WS_2$ on Si and ZnO on Si.

**(a)**

| $SiO_2$ Exciton | Value | Standard Error |
|---|---|---|
| $E_g(0)$ | 2.08 | 2.86E-03 |
| α | 3.78E-04 | 5.38E-05 |
| β | 166.86 | 81.48 |
| No. of Points | | 7 |
| Degrees of Freedom | | 4 |
| Reduced Chi-Sqr | | 2.00E-06 |
| Residual Sum of Squares | | 8.00E-06 |
| Adj. R-Square | | 0.997 |

**(b)**

| $SiO_2$ Trion | Value | Standard Error |
|---|---|---|
| $E_g(0)$ | 2.04 | 3.60E-03 |
| α | 6.21E-4 | 4.32E-05 |
| β | 472.66 | 0 |
| No. of Points | | 7 |
| Degrees of Freedom | | 5 |
| Reduced Chi-Sqr | | 2.38E-05 |
| Residual Sum of Squares | | 1.19E-04 |
| Adj. R-Square | | 0.971 |

**(c)**

| ZnO Exciton | Value | Standard Error |
|---|---|---|
| $E_g(0)$ | 2.08 | 2.53E-03 |
| α | 6.80E-04 | 3.04E-04 |
| β | 588.98 | 423.32 |
| No. of Points | | 7 |
| Degrees of Freedom | | 4 |
| Reduced Chi-Sqr | | 3.29E-06 |
| Residual Sum of Squares | | 1.32E-05 |
| Adj. R-Square | | 0.996 |

**(d)**

| ZnO Trion | Value | Standard Error |
|---|---|---|
| $E_g(0)$ | 2.02 | 2.51E-03 |
| α | 4.84E-4 | 3.20E-05 |
| β | 520.66 | 0 |
| No. of Points | | 7 |
| Degrees of Freedom | | 5 |
| Reduced Chi-Sqr | | 1.17E-05 |
| Residual Sum of Squares | | 5.84E-05 |
| Adj. R-Square | | 0.974 |

**Figure S5. Data Modelling Statistics for Exciton and Trion Energies of $WS_2$ on $SiO_2$ and $WS_2$ on ZnO Samples under the Varshni Relation.** **(a)** Fitting statistics for excitons in the $WS_2$ on $SiO_2$ sample under Varshni modelling. **(b)** Fitting statistics for trions in the $WS_2$ on $SiO_2$ sample under Varshni modelling. **(c)** Fitting statistics for excitons in the $WS_2$ on ZnO sample under Varshni modelling. **(d)** Fitting statistics for trions in the $WS_2$ on ZnO sample under Varshni modelling.

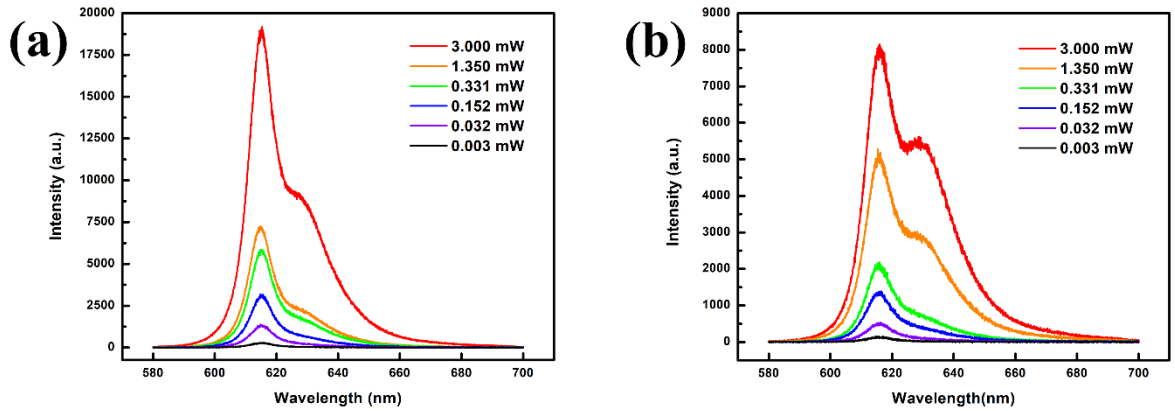


| | $WS_2$ on $SiO_2$ | | | | $WS_2$ on ZnO | | | |
|---|---|---|---|---|---|---|---|---|
| Excitation Power (mW) | $I_{Exciton}$ | $I_{Trion}$ | $I_{Trion}/I_{Exciton}$ | Ratio | $I_{Exciton}$ | $I_{Trion}$ | $I_{Trion}/I_{Exciton}$ | Ratio |
| 3.000 | 11851 | 8777 | 0.7406 | 2.506 | 4538 | 4976 | 1.0965 | 4.615 |
| 1.350 | 4981 | 2300 | 0.4618 | 1.562 | 2987 | 2743 | 0.9183 | 3.865 |
| 0.331 | 3949 | 1752 | 0.4437 | 1.501 | 1362 | 745 | 0.5470 | 2.302 |
| 0.152 | 2306 | 803 | 0.3482 | 1.178 | 967 | 417 | 0.4312 | 1.815 |
| 0.032 | 1001 | 295 | 0.2947 | 0.997 | 379 | 118 | 0.3113 | 1.310 |
| 0.003 | 203 | 60 | 0.2955 | 1.000 | 101 | 24 | 0.2376 | 1.000 |

**Figure S6. PL Spectra Evolution for the $WS_2$ on $SiO_2$ and $WS_2$ on ZnO Samples under Variable Excitation Powers.** **(a)** Spectra evolution for $WS_2$ on $SiO_2$ sample under 532 nm excitation power variation ranging from 0.003 mW to 3.000 mW. **(b)** Spectra evolution for $WS_2$ on ZnO sample under 532 nm excitation power variation ranging from 0.003 mW to 3.000 mW. Table below tallies the peak intensities for excitons, trions, trion-to-exciton metric ratio and ratio normalized against the lowest baseline excitation power (0.003 mW), for $WS_2$ on $SiO_2$ and $WS_2$ on ZnO samples respectively.